Supplement of Atmos. Chem. Phys., 18, 15975–16003, 2018
https://doi.org/10.5194/acp-18-15975-2018-supplement

Atmospheric Chemistry and Physics
Open Access

Supplement of

On the role of thermal expansion and compression in large-scale atmospheric energy and mass transports

Melville E. Nicholls and Roger A. Pielke Sr.

Correspondence to: Melville E. Nicholls (melville.nicholls@colorado.edu)

S1 A linearized one-dimensional solution for a thermal compression wave

The one-dimensional linearized momentum, thermodynamic and continuity equations, which allow thermal compression waves can be written as:

$$\frac{\partial u}{\partial t} + \frac{1}{\rho_0}\frac{\partial p'}{\partial x} = 0 \tag{S1}$$

$$\frac{\partial p'}{\partial t} - c^2\frac{\partial \rho'}{\partial t} = \frac{\gamma p_0}{c_\mathrm{p} T_0} Q_m \tag{S2}$$

$$\frac{1}{\rho_0}\frac{\partial \rho'}{\partial t} + \frac{\partial u}{\partial x} = 0 \tag{S3}$$

where u is the x-component of velocity, p' perturbation pressure from the base state, ρ' perturbation density, $c = \sqrt{\gamma R T_0}$ the speed of sound, $\gamma = c_\mathrm{p}/c_\mathrm{v}$, R the gas constant for dry air, and Q_m the hearting rate per unit mass. The basic state values of pressure, density, and temperature are p_0, ρ_0, and T_0, respectively. These reduce to a single equation for perturbation pressure:

$$\frac{\partial^2 p'}{\partial t^2} - c^2\frac{\partial^2 p'}{\partial x^2} = \frac{\gamma p_0}{c_\mathrm{p} T_0}\frac{\partial Q_\mathrm{m}}{\partial t} \tag{S4}$$

Consider a heating function $Q_m = U(t - t_0)Q_0 a^2/(x^2 + a^2)$ where the Heaviside unit function $U(t - t_0) = 1$ for $t > t_0$ and 0 for $t < t_0$. The equation can be solved for p' by taking Laplace and Fourier transforms, solving algebraically, and then taking inverse transforms to give:

$$p'(x,t) = \frac{\gamma p_0 Q_0 a}{c_\mathrm{p} T_0 c}\frac{1}{2}\left\{arctan\left(\frac{ct + x}{a}\right) + arctan\left(\frac{ct - x}{a}\right)\right\} \tag{S5}$$

It is straightforward to obtain solutions to the other variables (NP94a).

Figure S1 shows the solution for a heating rate of 1 J kg^{-1} s^{-1}, a=20 km, T_0=300 K, p_0=10^5 Pa at t=600 s. A narrow temperature increase occurs where the heating is large at x=500 km, but there is a very broad region of increased pressure. The solution has a wave-like character with the wave front, at around 200 km from the centre of the maximum heating, propagating at the speed of sound. There is divergence in the region of heating and convergence at the wave front. The passage of the wave front is characterized by a notable increase in pressure and relatively minor increases in density and temperature as the air is compressed.

The solution at 1200 s for a heating rate that is turned off at 600s is shown in Figure S2. Turning off the heating leads to a centre that is warmed and is less dense at 1200 s with only very small pressure perturbations remaining. Two wave-like anomalies are moving in opposite directions at the speed of sound. Since the internal energy per unit volume only depends on the pressure it can be seen that the internal energy perturbations given by $c_\mathrm{v}\, p'/R$, are propagating away from the heated region at the speed of sound. Even though the central region has warmed considerably there is no significant change in the internal energy per unit volume ($c_\mathrm{v}\rho T$) since there has been a large density decrease in the narrow heated region. Mass can be seen to be conserved since the density has increased slightly in the two wide compressed regions which are propagating away at the speed of sound. Therefore, this very simple 1D solution shows a significant redistribution of internal energy and mass occurring at the speed of sound.

There are two energy conservation equations that can be derived from equations S1-S3. The internal energy perturbation equation is

$$\frac{\partial}{\partial t}\left(\frac{c_\mathrm{v} p'}{R}\right) + \frac{\partial}{\partial x}\left(c_\mathrm{p}\rho_0 T_0 u\right) = Q_\mathrm{v} \tag{S6}$$

where Q_{v} is the heating rate per unit volume $(\rho_0 Q_{\mathrm{m}})$. The wave energy equation is

$$\frac{\partial}{\partial t}\left(\rho_0 \frac{u^2}{2} + \frac{p'^2}{2\rho_0 c^2}\right) + \frac{\partial}{\partial x}(up') = \frac{Rp'}{c_{\mathrm{p}}\, p_0} Q_{\mathrm{v}} \tag{S7}$$

The wave energy in Eq. S7 is composed of kinetic energy and wave potential energy (e.g. Phillips, 1990). Figure S3 portrays the two expressions for internal energy perturbation and wave energy for the thermal compression wave shown in Fig. S2. It can be seen that the internal energy perturbation is four orders of magnitude larger than the wave energy. In this study we are concerned with how expansion of air due to a heat source and the resultant compression of the surrounding air leads to a transfer of total energy at the speed sound. If solutions to the nonlinear equations were obtained for this problem the total energy would consist of internal energy plus kinetic energy with the latter being an extremely small contribution. The total energy would to a good approximation be equal to the internal energy and the solutions for small perturbations would be similar to these we have obtained for the linearized equations. As this simple linearized solution illustrates it is important not to confuse the transfer of total energy by thermal compression waves with the transfer of wave energy.

S2 A thought experiment demonstrating internal energy transfer is different than convective heat transfer

Another perspective on internal energy transfer is gained by considering the thought experiment shown in Figure 3. An ideal gas in an insulated container is separated into two parts, gas 1 and gas 2, by a movable frictionless partition. Consider uniformly heating gas 1 on the left side of the container. This will cause the temperature and pressure to increase. Gas 1 will expand and the movable partition will move to the right compressing gas 2. If the heating is discontinued the partition will come to an equilibrium position, as shown in Fig. 3b, such that the pressure in gas 2 equals the pressure in gas 1. The temperature of gas 2 will have increased due to compression, but will be considerably less than that of gas 1. Since the internal energy per unit volume $(c_{\mathrm{v}}p/R)$ is only a function of pressure, it will be the same in gas 2 as in gas 1. Obviously, since gas 1 now occupies a larger volume than gas 2 it will have a larger net internal energy.

The compression of gas 2 is a fast response occurring at the speed of sound. As the partition moves from left to right it imparts momentum to the adjacent molecules in gas 2 causing a wave of compression to travel through gas 2 at the speed of sound, which reflects backwards and forwards off the right lateral boundary and the middle partition. Now consider removing the partition. If the two gases were then mixed by mild stirring this wouldn't impart significant internal energy (stirring a gas will not increase its temperature by much), and the pressure would remain essentially the same. As far as the internal energy in a control volume in gas 2 is concerned, the internal energy increased during the compression stage. After the mixing stage, even though the control volume contains warmer air than it did at the end of the compression stage, the amount of internal energy within it has not changed since the pressure is the same. Note that the density of the gas in the control volume that was larger than the density in gas 1 will decrease during this mixing phase as the density throughout the container becomes uniform.

Convective heat transfer is considered to be the transfer of heat from one place to another by the movement of fluids. It is common in meteorology to describe heat as being advected from one place to another, whereby it is meant that when relatively warm air moves into a region it constitutes a "heat transfer". This interpretation is at the heart of the decomposition made in Eq. 3. From this perspective the heat transport from left-to-right in the thought experiment depicted in Fig. 3 took place in the second stage when air was mixed and the air in the control volume became notably warmer. However, as has been explained, this did not constitute a total energy transfer, which occurred earlier in stage 1 during the compression of gas 2.

S3 Results for Experiment 1B

Early in the simulation at 10 s (Fig. S5) there are significant differences with the fully compressible solution (Fig. 4). For instance the potential temperature perturbation in the heat source region is noticeably less than for the fully compressible case. This is probably because there is already upward motion at the center of the heat source leading to some adiabatic cooling, which does not exist in the case of the fully compressible simulation. Also the surface pressure has already begun to decrease (Fig. S5b) and there is no expansion of the air evident in the horizontal and vertical velocity fields. Instead of showing expansion the circulation has an inflow at low levels and outflow at the upper region of the heat source with a deep updraft at the center. Figure S6 shows the density perturbation at 40 s, u at 80 s, and vertical velocity at 120 s, that can be compared with the corresponding frames in Fig. 3 and 4 for the compressible simulation. The density perturbation is larger in magnitude than for the fully compressible case. Also, the inflow is stronger and the outflow weaker, which is consistent with an outflow velocity associated with expansion of the heated air for the compressible case superimposed onto the buoyancy driven circulation. This simulation at 120 s has developed a more extensive subsidence region surrounding the updraft. Figure S7 at 15 min can be compared to the compressible case in Fig. 7. Despite the differences noted early in the simulations, at this time the results are virtually identical. One discernable difference is that the pressure perturbation at the top of the heat source for the compressible case (Fig. 7b) is slightly higher (Fig. S7b).

S4 Results for Experiment 2C

Figure S8 shows a horizontal section of the surface pressure perturbation and a vertical section through the centre of the domain of the total energy perturbation for Experiment 2C, which does not include the Coriolis term. Comparing Fig. S8a and b, with Fig. 8b and d, it can be seen that the inclusion of the Coriolis force radically alters the pressure field and distribution of total energy. Far less total energy occurs over the land surface for this simulation and it is being redistributed much further offshore. Time series for this simulation shown in Figure S9 illustrate how much larger the total energy is over the ocean than over the land at the end of the 9 h simulation. There is also significantly more mass transported offshore for this experiment than for Experiment 2A (cf. Fig. 10d).

References

Phillips, N. A.: Dispersion Processes in Large-Scale Weather Prediction. WMO-700, 126 pp., 1990.

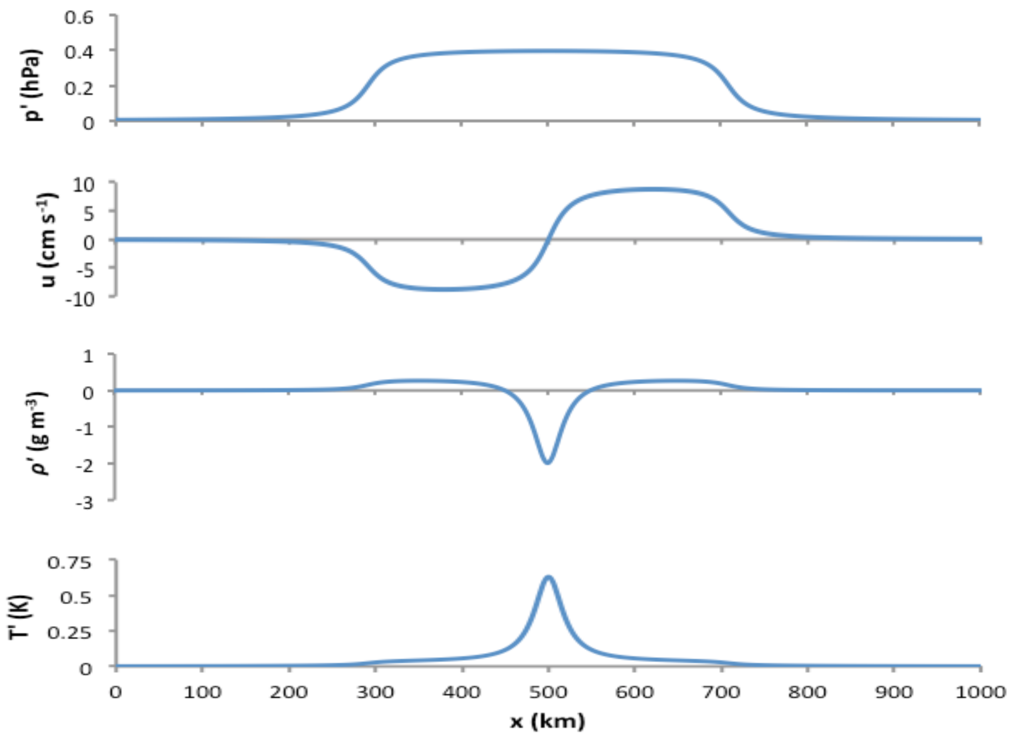

Figure S1. Solution for a 1D thermally generated compression wave at t=600 s.

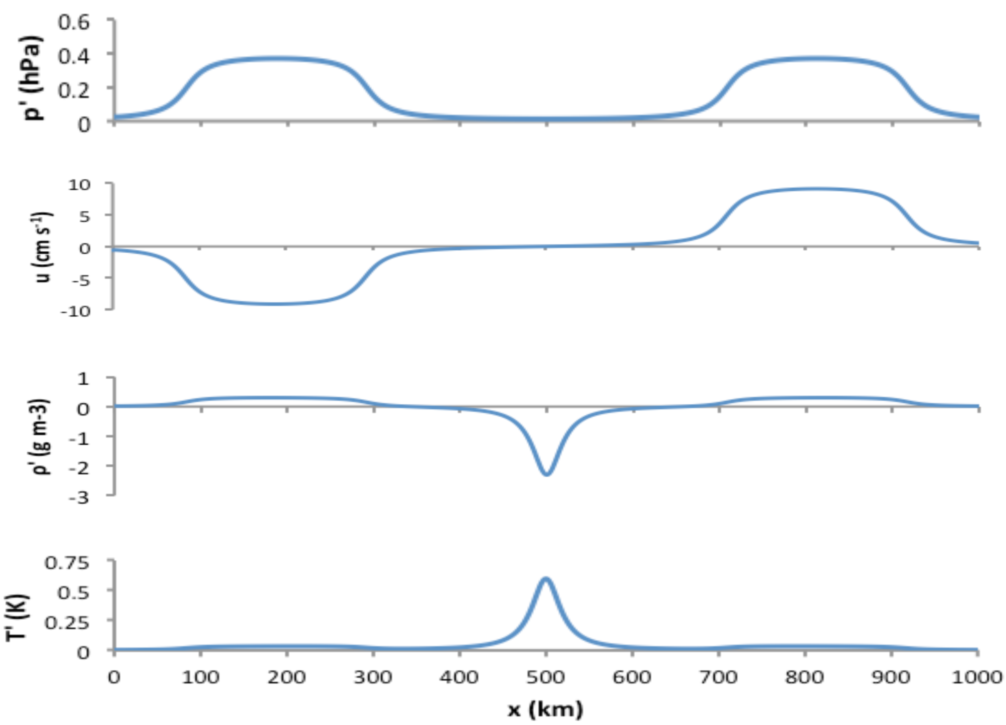

Figure S2. Solution for a 1D thermally generated compression wave at t=1200 s. with the heating turned off at t=600 s.

(a) Total energy $\left(\frac{c_V p'}{R}\right)$

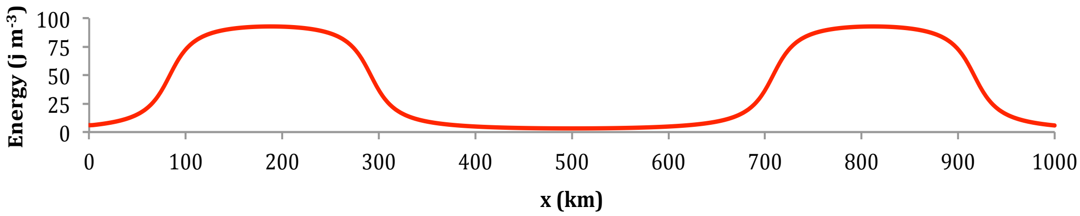

(b) Wave energy $\left(\rho_0 \frac{u^2}{2} + \frac{p'^2}{2\rho_0 c^2}\right)$

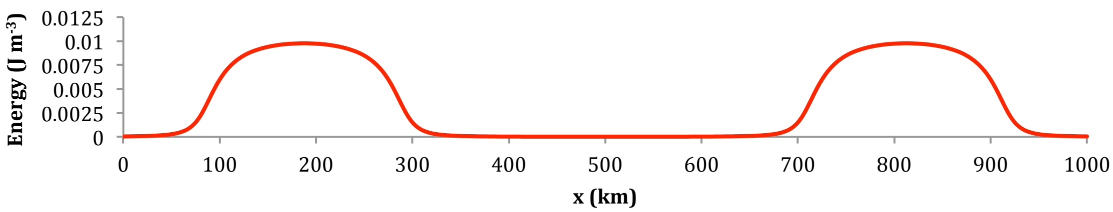

Figure S3. Total energy and wave energy for a 1D thermally generated compression wave at t=1200 s, with the heating turned off at t=600 s. (a) Total energy. (b) Wave energy.

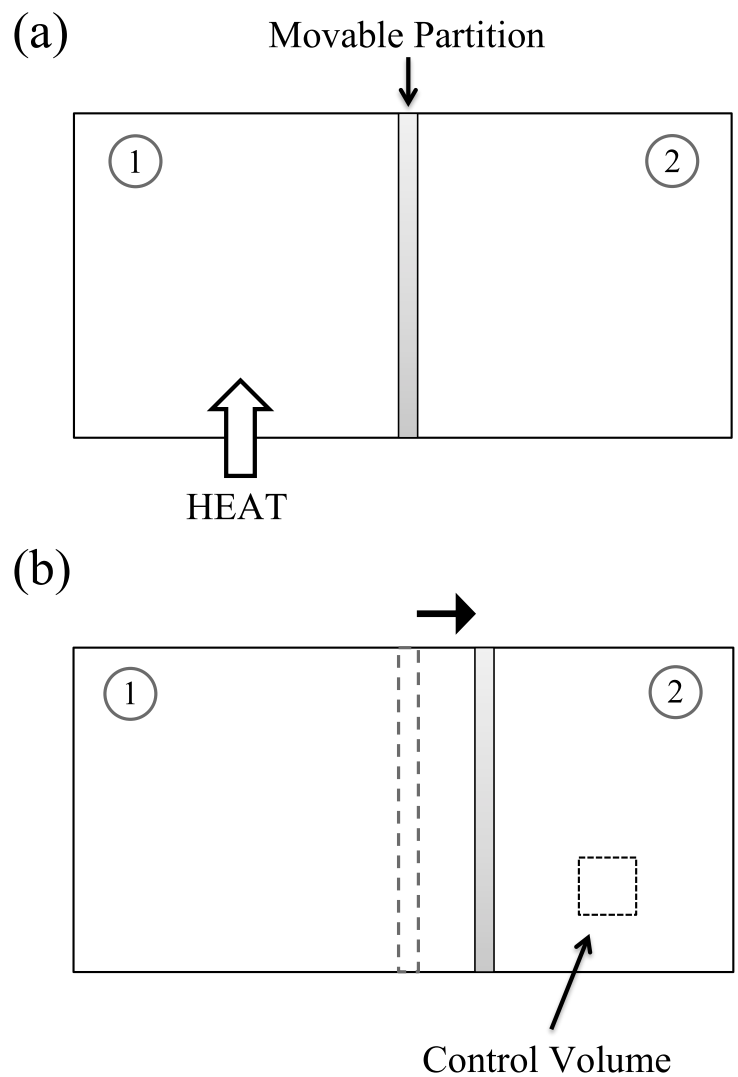

Figure S4. Schematic of a thermally insulated gas divided by a movable partition. (a) Initial state. (b) After heat input in chamber 1.

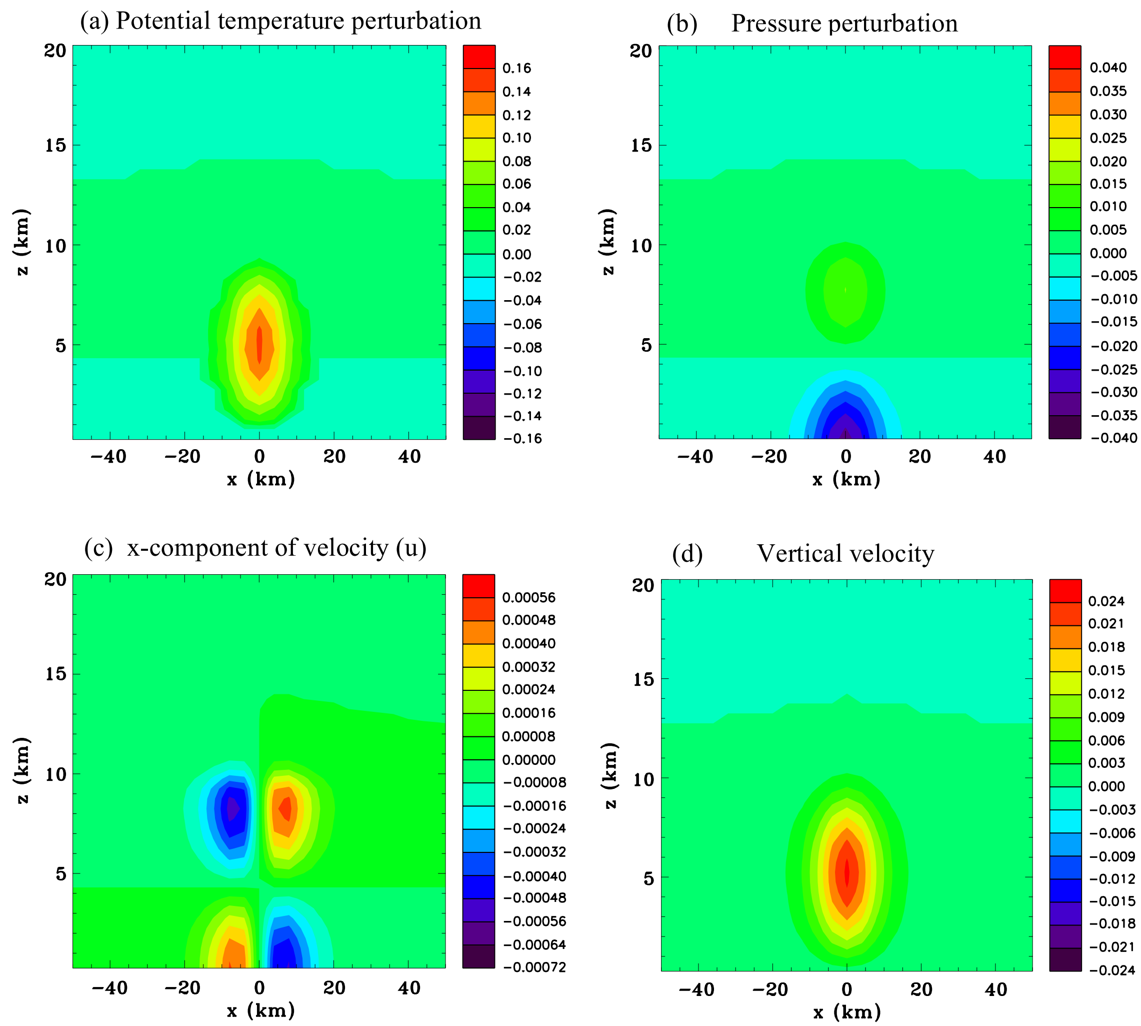

Figure S5. Vertical sections for the convective scale heat source without compression waves, Experiment 1B, at t=10 s. (**a**) Potential temperature perturbation (K), (**b**) pressure perturbation (hPa), (**c**) x-component of velocity (m s^{-1}). and (**d**) vertical velocity (m s^{-1}).

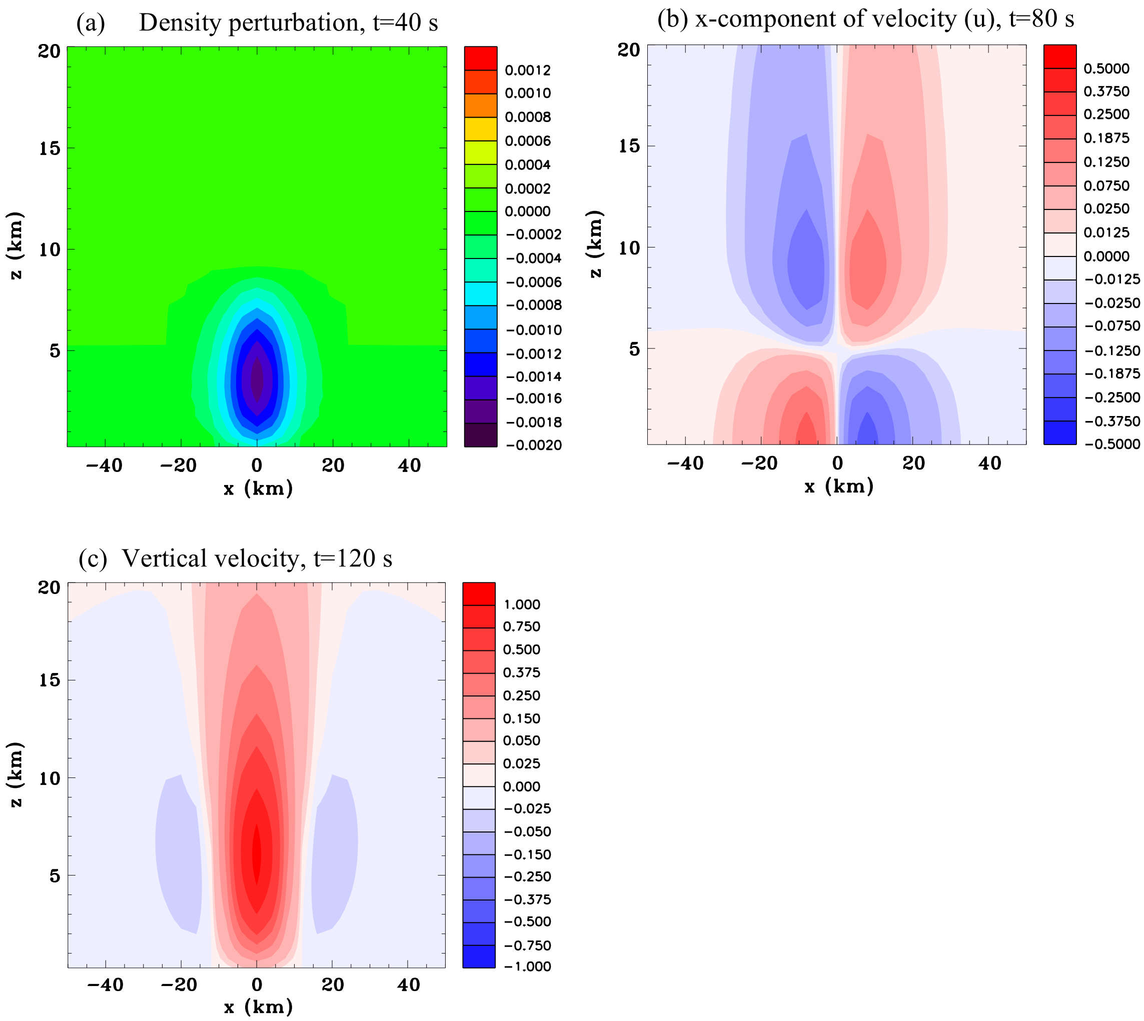

Figure S6. Vertical sections for the convective scale heat source without compression waves, Experiment 1B. (**a**) Density perturbation (kg m^{-3}), at t=40 s (**b**) x-component of velocity (m s^{-1}), at t=80 s and (**c**) vertical velocity (m s^{-1}), at t=120 s.

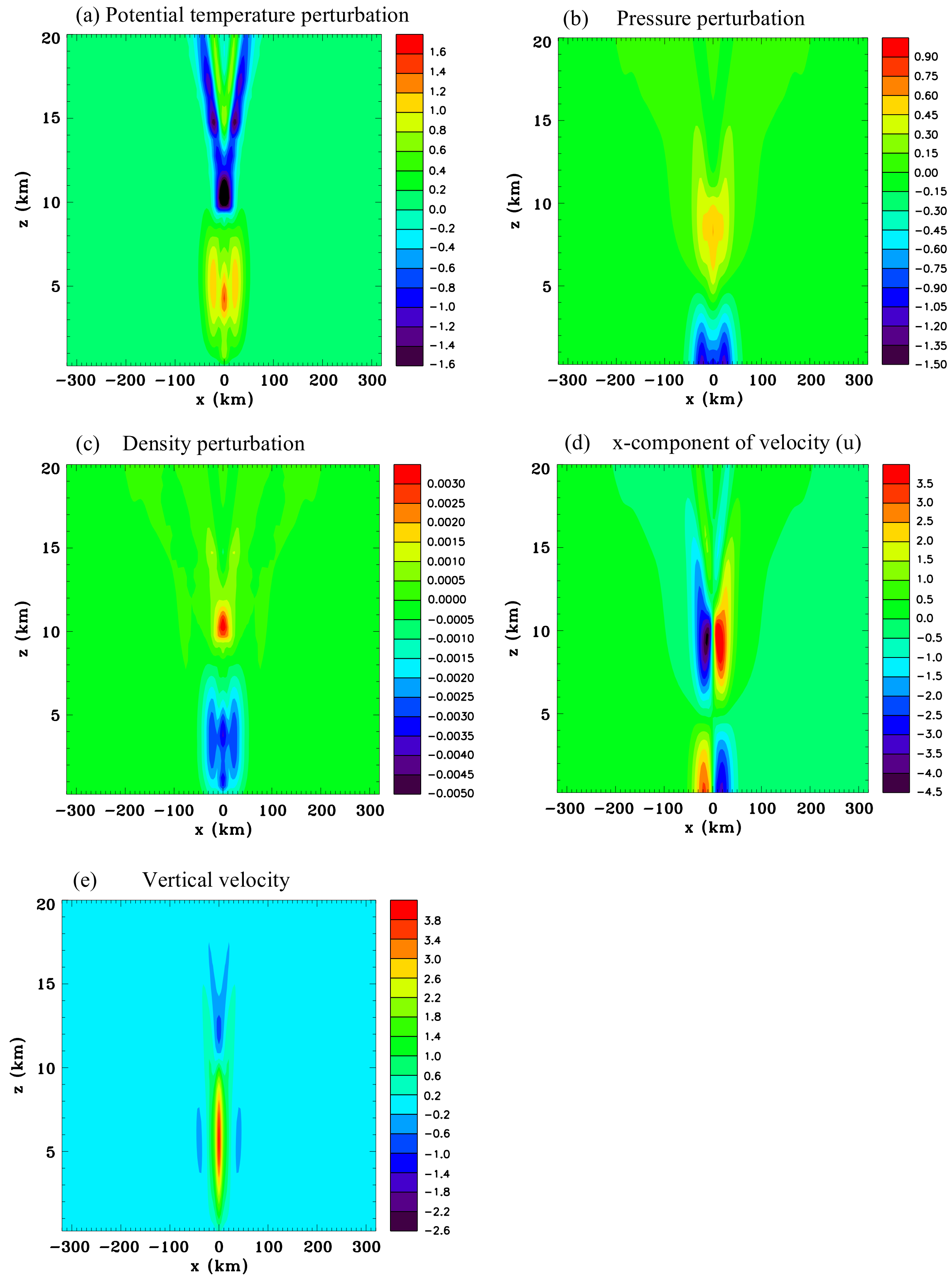

Figure S7. Vertical sections for the convective scale heat source without compression waves, Experiment 1B, at t=15 minutes. (**a**) Potential temperature perturbation (K), (**b**) pressure perturbation (hPa), (**c**) density perturbation (kg m^{-3}), (**d**) x-component of velocity (m s^{-1}), and (**e**) vertical velocity (m s^{-1}).

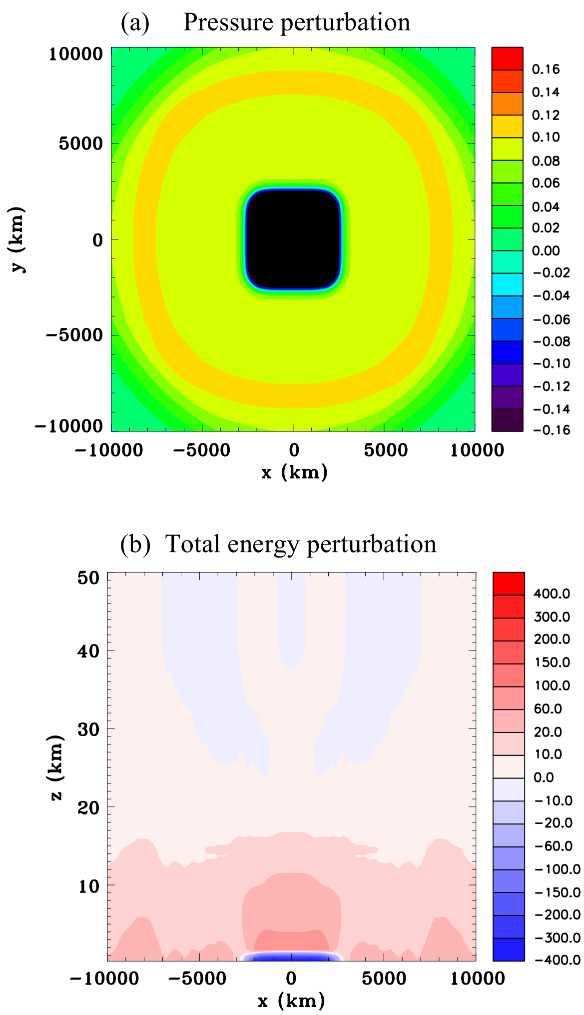

Figure S8. Continent-scale heat source without the Coriolis force, Experiment 2C, at t=9 h. (**a**) Surface pressure perturbation (hPa), and (**b**) vertical section of the total energy perturbation (J m^{-3}).

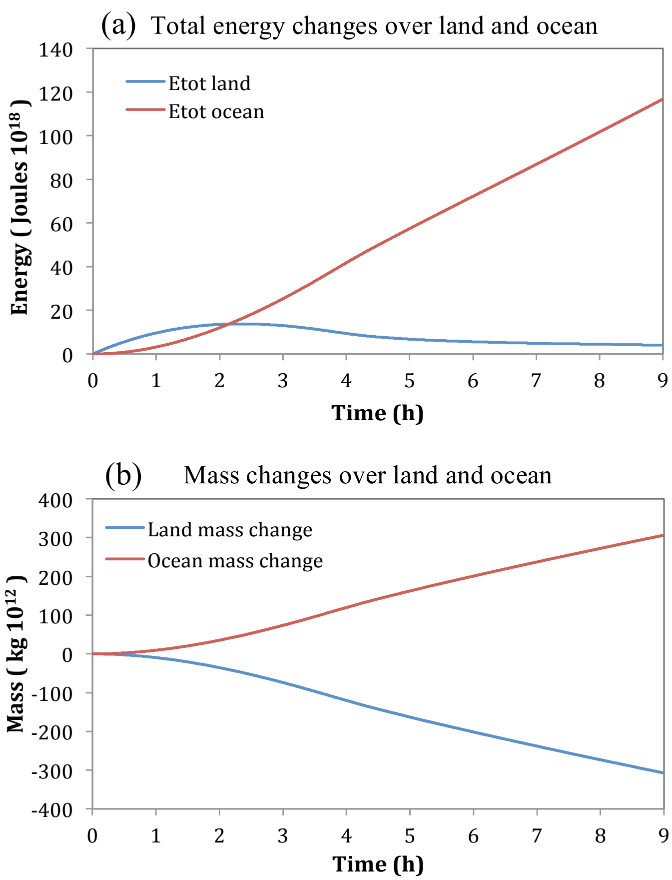

Figure S9. Time series for the square continent scale heating without Coriolis force, Experiment 2C. (**a**) Total energy changes over the land and ocean (Joules $\times 10^{18}$), and (**b**) mass changes over the land and ocean (kg $\times 10^{12}$).